

Improving Robotic Manipulation with Efficient Geometry-Aware Vision Encoder

An Dinh Vuong¹, Minh Nhat Vu², Ian Reid¹

Abstract—Existing RGB-based imitation learning approaches typically employ traditional vision encoders such as ResNet or ViT, which lack explicit 3D reasoning capabilities. Recent geometry-grounded vision models, such as VGGT [1], provide robust spatial understanding and are promising candidates to address this limitation. This work investigates the integration of geometry-aware visual representations into robotic manipulation. Our results suggest that incorporating the geometry-aware vision encoder into imitation learning frameworks, including ACT and DP, yields up to 6.5% improvement over standard vision encoders in success rate across single- and bi-manual manipulation tasks in both simulation and real-world settings. Despite these benefits, most geometry-grounded models require high computational cost, limiting their deployment in practical robotic systems. To address this challenge, we propose eVGGT, an efficient geometry-aware encoder distilled from VGGT. eVGGT is nearly 9× faster and 5× smaller than VGGT, while preserving strong 3D reasoning capabilities. Code and pretrained models will be released to facilitate further research in geometry-aware robotics.

I. INTRODUCTION

Imitation learning (IL) offers a promising solution for enabling robots to acquire manipulation skills directly from rich expert demonstrations that capture world coordination and contact dynamics [2], [3]. Since many manipulation tasks require precise geometric understanding and alignment, effective 3D reasoning is essential for success [4]. Nevertheless, most RGB-based IL approaches employ 2D vision encoders such as ResNet or ViT, which lack explicit modeling of global geometric structure [5]. This limitation poses significant challenges for developing intelligent robotic systems [6], underscoring the need for robust vision encoders that can capture 3D spatial relationships among objects [7].

Recent advances in visual geometry [1], [8], [9] have enabled significant progress in robotic applications such as localization and mapping [8]. These feed-forward neural networks take uncalibrated images as input and jointly estimate depth maps, point maps, feature tracks, and camera poses [10]. The strong geometric reasoning capabilities of these models can effectively overcome the lack of 3D awareness in existing 2D-based IL methods [7]. Despite impressive performance, their large architectures often result in slow inference [11], limiting their applicability in real-time robotic systems [10]. We address this gap by proposing a lightweight geometry-aware vision encoder for robotic manipulation. Thanks to our proposed vision encoder, we can efficiently leverage geometric representations in robotic manipulation,

resulting in up to 6.5% improvement on standard IL baselines, as illustrated in Fig. 1.

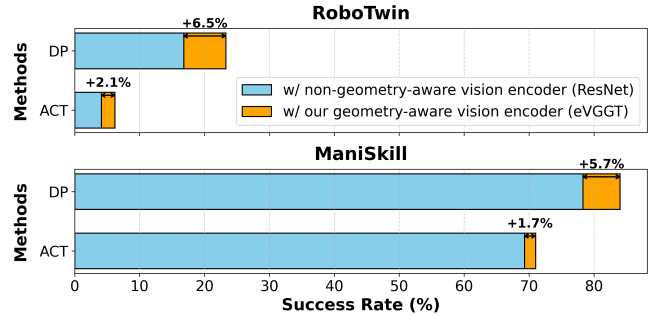


Fig. 1. We investigate replacing traditional 2D vision encoders in robotic manipulation with geometry-grounded methods to capture 3D global context better. Results demonstrate that incorporating our geometry-aware vision encoder improves performance by up to 6.5%.

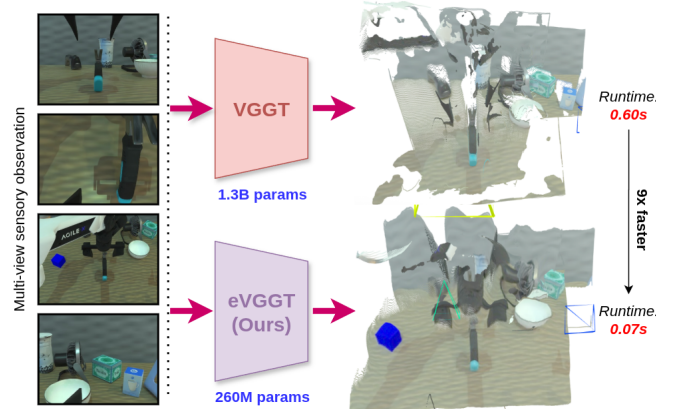


Fig. 2. To facilitate transferring knowledge from geometry-aware networks, we propose a lightweight variant, **eVGGT**, which is 5× smaller and 9× faster while maintaining strong geometric reasoning capabilities.

Knowledge distillation is a well-established method for transferring knowledge from large models to smaller ones [12], [13], enabling resource-efficient deployment on hardware-constrained robots with minimal accuracy loss [14]. A key challenge, however, is that student models often overfit to the teacher’s outputs [15]. To mitigate this, we revisit data augmentation [16], which increases input diversity and allows the student model to capture more of the teacher’s knowledge, leading to better generalization [17]. Using this training scheme, we present an efficient visual geometry encoder that is nearly 9× faster and 5× smaller than the original VGGT [1] while preserving its effectiveness in reconstructing 3D geometric structures, as shown in Fig. 2.

Building on our proposed geometry-aware vision encoder, we integrate it into IL by transferring its latent represen-

¹Department of Computer Vision, Mohammed bin Zayed University of Artificial Intelligence, UAE an.vuong@mbzuai.ac.ae

²AIT Austrian Institute of Technology GmbH, Austria

tations into the training of robotic policies. Our approach is simple yet effective: we replace traditional 2D vision encoders’ latent space with that of our proposed geometry-aware encoder in standard IL baselines. We evaluate our method across different robotic manipulation simulators, including both bi-manual tasks (RoboTwin [18]) and single-arm tasks (ManiSkill [19]), demonstrating its broad applicability. In summary, our contributions are as follows:

- We introduce a lightweight geometry-aware vision encoder, distilled from the high-performing VGGT network, while preserving its 3D reconstruction capability.
- We present a simple yet effective approach to integrate geometry-aware representations into robotic policies by leveraging our encoder’s latent space.
- Experiments in simulation and on a real robot system suggest that our encoder effectively captures global 3D context and significantly improves manipulation success.

II. RELATED WORK

Visual Representations for Imitation Learning. Understanding visual information is crucial in IL, as observations provide dynamic information of expert behavior [20]. Traditionally, vision encoders such as ResNet and ViT have been widely employed [21]–[24], but these encoders often fail to model object dynamics from static images [5]. To better capture environmental dynamics, some approaches utilize intermediate visual representations, including bounding boxes [25], object flow [26], or keypoints [27]. However, these object-centric representations still lack global context and, therefore, struggle to generalize tasks involving previously unseen objects [28]. Point clouds or other 3D geometric representations, such as Gaussian splatting [7], have also been employed in robotic manipulation [5], [29], [30], as they directly encode 3D spatial structures and provide a more comprehensive understanding of the scene [31]. In practice, these 3D structure methods often depend on external processing or foundation models to achieve strong performance [30], and scaling them to match the accessibility of RGB observations in real robotic systems remains difficult [5]. To overcome these challenges, we propose leveraging high-performance visual geometry networks [1] to develop an end-to-end approach, enabling direct application to robotic policies without dependence on external processing.

Imitation Learning for Robotic Manipulation. IL is a promising approach for enabling generalizable manipulation behaviors using large-scale datasets [24]. Given the difficulties of precisely determining object states in real-world environments [21], 2D image-based IL methods such as ACT [22] and DP [23] have emerged as effective and popular solutions in the field [19]. More recent IL approaches have shifted towards 3D-based representations to capture the structure of the environment better [18], [32]. By addressing efficiency in high-dimensional control, DP3 [30] has proven to be among the most effective methods. Another prospective direction is the development of large-scale foundation models for multi-task generalist policies, such as RDT [24].

However, these pretrained models often remain inefficient and require substantial fine-tuning to learn new tasks [27].

Knowledge Distillation for Efficiency. Knowledge distillation has emerged as an effective tool for compressing and accelerating neural networks [33], [34], in which a student model is trained to mimic a teacher model using supervision signals that may include latent representations [35] or model outputs [36]. Few studies have explored knowledge distillation in the context of geometry-grounded vision models [11], and these works primarily focus on distilling VGGT to leverage its geometric reasoning for downstream tasks such as geometry-aware video generation [37] or vision-language modeling [38]. In contrast, we leverage knowledge distillation to improve the efficiency of VGGT. A known challenge is that the student model can overfit to the teacher’s behavior [15], necessitating the use of regularization techniques to enhance generalization [39]. To address this, an effective approach is to apply data augmentation during distillation, which can increase input diversity and expose richer teacher knowledge to the student [17].

III. METHOD

We present a method for transferring knowledge from VGGT [1] to robotic manipulation. Since VGGT is large and computationally expensive, we propose a knowledge-distilled variant that improves efficiency while retaining geometric reasoning. This section is organized as follows: we first provide preliminaries on VGGT, then describe our knowledge distillation framework, and finally explain how the distilled encoder is integrated into robotic manipulation through imitation learning.

A. Preliminaries on VGGT

VGGT is a vision transformer trained on extensively large datasets and exhibits strong geometric reasoning capabilities compared to several other geometry-grounded networks [8]–[10]. An overview of VGGT is depicted in Fig. 3.

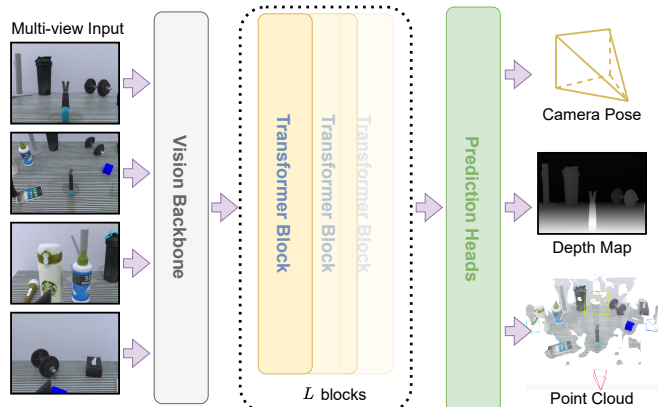


Fig. 3. **VGGT architecture.** VGGT is a transformer-based vision encoder that produces geometry-aware features from multi-view input.

Given a set of N input images $\{I_1, I_2, \dots, I_N\}$, VGGT first tokenizes into patches of size $P \times P$ using a fine-tuned DINOv2-ViT-L backbone [40], producing frame token sequences $\{\ell_1, \ell_2, \dots, \ell_N\}$. To facilitate camera parameter

prediction, special *camera* tokens ℓ_i^c and *register* tokens ℓ_i^r are added to each frame token sequence, allowing the model to distinguish the first frame from subsequent frames [41]. The final frame representation is denoted as $\mathbf{z}_i = (\ell_i, \ell_i^c, \ell_i^r)$, and the collection of frame features is $\mathcal{Z} = \{\mathbf{z}_1, \mathbf{z}_2, \dots, \mathbf{z}_N\}$.

The feature set \mathcal{Z} is then fed into a transformer network comprising L transformer blocks. Each block employs *Alternating-Attention*, which alternates between global attention over the entire sequence \mathcal{Z} and frame-wise self-attention applied to the individual frame token sequences $\mathbf{z}_i, \forall i \in [1, N]$. The resulting output tokens $\hat{\mathbf{z}}_i$ for each frame can then be utilized either by *i*) a camera head, implemented as a transformer for estimating camera poses, or *ii*) Dense Prediction Transformer (DPT) heads [42], which generate geometric outputs including depth maps and point clouds.

The main computational bottleneck of VGGT comes from its transformer module, consisting of $L = 24$ blocks, which limits its practicality for robotic tasks. Moreover, VGGT is originally designed for high-resolution images, while most robotic settings leverage lower-resolution images to maintain efficiency and scalability [43]. Following the scaling practice [44], we propose a compressed VGGT architecture that suits the lower-resolution images typical in these robot settings, described in Sec. III-B.

B. Efficient VGGT using Knowledge Distillation

Redesigned Architecture. To improve the efficiency of VGGT, we reduce the number of transformer blocks from $L = 24$ to $L = 4$. The choice of 4 blocks is motivated by VGGT’s design, where the DPT heads extract and fuse features from four intermediate transformer blocks to predict dense depth and point maps. To maintain compatibility with the teacher VGGT model, we preserve the structure of the prediction heads, making 4 the minimal number of blocks that allows supervision of the student’s intermediate representations. In addition, since robotic environments typically operate on low-resolution images, we follow the scaling rules of ViT models [44] and replace the DINOv2-ViT-L backbone with the smaller DINOv2-ViT-S. These modifications result in a lightweight VGGT that preserves geometric reasoning while substantially lowering computational cost. We refer to this proposed architecture as **eVGGT** (efficient VGGT), which serves as the student model trained under a pretrained VGGT teacher model. Importantly, the student relies only on the teacher’s outputs, requiring no ground-truth labels, making eVGGT applicable to diverse robotic environments.

Training Knowledge Distillation. The outputs of the VGGT model for each image I_i include: *i*) camera parameters θ_i , *ii*) depth map \mathbf{D}_i , and *iii*) point cloud \mathbf{P}_i . Denote \ast^{std} and \ast^{tch} as the outputs of the student and teacher models, respectively. Following [34], the knowledge distillation loss is defined as:

$$\mathcal{L}_{\text{distill}} = \sum_{i=1}^N \left(\|\theta_i^{\text{std}} - \theta_i^{\text{tch}}\|^2 + \|\mathbf{D}_i^{\text{std}} - \mathbf{D}_i^{\text{tch}}\|^2 + \|\mathbf{P}_i^{\text{std}} - \mathbf{P}_i^{\text{tch}}\|^2 \right). \quad (1)$$

Empirically, we observe that the depth maps predicted by the student model trained with Eq. (1) exhibit noticeable

noise and lack smoothness. This problem is mainly due to the difference in scale between the student backbone (DINOv2-ViT-S) and the teacher backbone (DINOv2-ViT-L) [45]. To address this, we incorporate a gradient loss following [1]:

$$\mathcal{L}_{\text{grad}} = \sum_{i=1}^N \left(\|\nabla_x \mathbf{D}_i^{\text{std}} - \nabla_x \mathbf{D}_i^{\text{tch}}\|_1 + \|\nabla_y \mathbf{D}_i^{\text{std}} - \nabla_y \mathbf{D}_i^{\text{tch}}\|_1 \right), \quad (2)$$

where ∇_x and ∇_y are the gradients along the x and y axes of the depth map. The final training loss is $\mathcal{L} = \mathcal{L}_{\text{distill}} + \mathcal{L}_{\text{grad}}$.

Data Augmentation. Since data augmentation can improve the generalization of the student model [17], we augment only the student’s input images, keeping the teacher’s inputs unchanged for stable supervision. Following [1], we adopt three augmentations: *i*) color jitter (brightness, contrast, saturation, hue), *ii*) random grayscale conversion with probability 0.3, and *iii*) Gaussian blur (a 3×3 kernel, $\sigma \in [0.1, 2.0]$). These commonly used augmentations have proven effective for 3D reconstruction [46]. As shown in Sec. IV, this simple strategy can improve 3D reconstruction quality significantly.

C. Integration into Robotic Policies

To leverage the geometric reasoning capabilities of eVGGT in robotic policy learning, we replace the standard vision encoders in existing IL with a pretrained and frozen eVGGT, as described in Sec. III-B. This frozen design choice enables direct use of 3D spatial representations without the need for additional task-specific fine-tuning, which is more suitably handled by the policy heads [47]. We remove eVGGT’s prediction heads and extract only the latent geometric features from the transformer blocks (Fig. 3), substantially reducing computational cost. Adaptive MLPs are then applied to project these latent features to match the input dimensionality of the policy heads.

We focus on two representative IL approaches: *i*) ACT [22], a transformer-based policy, and *ii*) DP [23], a diffusion model-based policy. The integration of our eVGGT encoder into these policies is quite straightforward, as illustrated in Figs. 4 and 5.

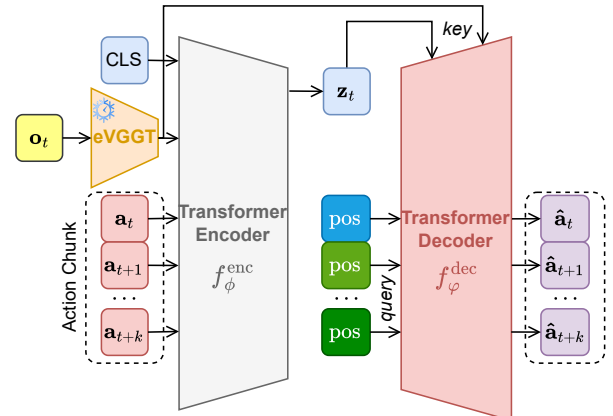


Fig. 4. **Integration of eVGGT into ACT.** eVGGT provides geometry-aware visual features for both the encoder and decoder of ACT.

Action Chunking with Transformer (ACT). To enforce temporal smoothness in predicted actions, ACT predicts the

next chunk of k actions, $\mathbf{a}_{t:t+k}$, from the current observation \mathbf{o}_t (which may include multiple views) at timestep t . This is implemented using a transformer-based conditional VAE comprising two components: *i*) a transformer encoder $f_\phi^{\text{enc}}(\mathbf{z}_t \mid \mathbf{o}_t, \mathbf{a}_{t:t+k})$ and *ii*) a transformer decoder $f_\phi^{\text{dec}}(\hat{\mathbf{a}}_{t:t+k} \mid \mathbf{z}_t, \mathbf{o}_t)$, where \mathbf{z}_t is a latent variable.

The observation \mathbf{o}_t is first embedded using eVGGT to produce a latent feature $\mathbf{y}_t = \text{eVGGT}(\mathbf{o}_t)$ with geometric reasoning capabilities, which is then incorporated into both the encoder and decoder. Specifically, the transformer encoder maps the sequence $[\text{CLS}, \mathbf{y}_t, \mathbf{a}_{t:t+k}]$ to the latent variable \mathbf{z}_t extracted from the CLS token, while the transformer decoder takes the sequence $[\mathbf{z}_t, \mathbf{y}_t]$ as input *key* and generates the predicted action chunk $\hat{\mathbf{a}}_{t:t+k}$.

Diffusion Policy (DP). DP formulates the policy as a denoising diffusion probabilistic model (DDPM) [48], following the same principle as ACT by predicting a sequence of actions $\mathbf{A}_t = \mathbf{a}_{t:t+T_a}$ from a sequence of observations $\mathbf{O}_t = \mathbf{o}_{t-T_o:t}$, where T_o and T_a denote the respective chunk sizes as defined in [23]. The process consists of two stages: *i*) forward process that gradually adds noise to the action sequence, and *ii*) a reverse process that learns to recover the original action sequence, conditioning on the current observations.

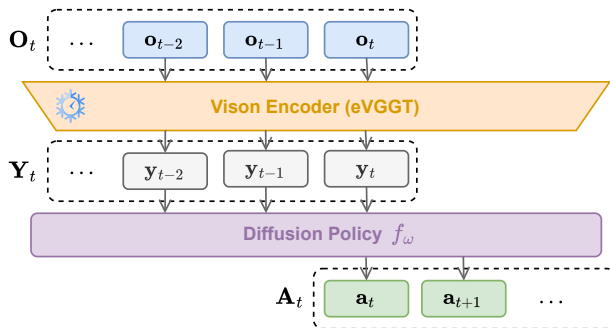


Fig. 5. **Integration of eVGGT into DP.** eVGGT encodes observations to transfer geometric representation for the guided diffusion process.

In the forward process, the clean action chunk \mathbf{A}_t is gradually perturbed with Gaussian noise according to a predefined schedule. At each diffusion step $k \in \{1, \dots, K\}$, the noisy data $\mathbf{A}_t^{(k)}$ is obtained as follows:

$$\mathbf{A}_t^{(k)} = \sqrt{\bar{\alpha}_k} \mathbf{A}_t^{(0)} + \sqrt{1 - \bar{\alpha}_k} \boldsymbol{\epsilon}, \quad \boldsymbol{\epsilon} \sim \mathcal{N}(\mathbf{0}, \mathbf{I}), \quad (3)$$

where $\bar{\alpha}_k = \prod_{j \leq k} \alpha_j$ with α_j defined by the variance schedule [48], and $\mathbf{A}_t^{(0)}$ denotes as the original action chunk. In the reverse process, the observation \mathbf{O}_t is first encoded into a global-context embedding $\mathbf{Y}_t = \text{eVGGT}(\mathbf{O}_t)$, which provides informative 3D guidance for denoising. Starting from noisy $\mathbf{A}_t^{(k)}$, we iteratively denoise toward $\mathbf{A}_t^{(0)}$ by:

$$\mathbf{A}_t^{(k-1)} = \frac{1}{\sqrt{\alpha_k}} \left(\mathbf{A}_t^{(k)} - \frac{1 - \alpha_k}{\sqrt{1 - \bar{\alpha}_k}} f_\omega(\mathbf{A}_t^{(k)}, \mathbf{Y}_t, k) \right) + \sigma_k \mathbf{z}, \quad (4)$$

where $\mathbf{z} \sim \mathcal{N}(\mathbf{0}, \mathbf{I})$, f_ω denotes the transformer-based denoising network [23], and σ_k represents the standard deviation of the Gaussian noise in the reverse process [48].

IV. EXPERIMENT

We perform experiments to evaluate the effectiveness of our proposed eVGGT for robotic manipulation. Specifically, we aim to answer the following questions:

- **Q1:** To what extent does our geometry-aware eVGGT encoder improve robotic manipulation performance?
- **Q2:** What information does eVGGT capture that contributes to manipulation success, and how efficient is it?
- **Q3:** Can our approach transfer effectively from simulation to the real world?

A. Robotic Manipulation in Simulation

Setup. We evaluate the impact of eVGGT on IL policies for robotic manipulation. On RoboTwin [18], we consider six representative tasks from the 50-task benchmark: *Beat Block Hammer*, *Adjust Bottle*, *Lift Pot*, *Place Burger Fries*, *Press Stapler*, and *Handover Mic*. In the original benchmark [18], models are trained on 50 *clean* demonstrations, where scenes contain a single object, and evaluated on *randomized* scenes, which include clutter. We argue that this setting is unsuitable, as cluttered scenes provide richer information about object dynamics [28]. Therefore, we modify the protocol to train on 50 *randomized* demonstrations (Seen) for 10K iterations and evaluate on both the seen setting and the *clean* setting (Unseen). For ManiSkill [19], we train all policies for 30K iterations on three tasks: *Pick Cube*, *Push Cube*, and *Stack Cube*, following the setup in [24], [49]. All experiments are conducted on an NVIDIA RTX 4090 GPU (24GB), with each robotic task completed within 12 hours.

Baselines. We compare our methods, ACT+eVGGT and DP+eVGGT, which use eVGGT as the geometry-aware vision encoder (Sec. III-B), against RDT [24], a strong IL baseline capable of scaling to match state-of-the-art VLA models, as well as the vanilla ACT [22] and DP [23]. On RoboTwin, we also include DP3 [30] as a baseline, while excluding it on ManiSkill due to the absence of 3D point cloud input in the standard setup [19]. Performance is evaluated in terms of success rate, following the implementations provided in the RoboTwin and ManiSkill simulators.

Results on RoboTwin. On RoboTwin, integrating eVGGT into existing IL frameworks yields substantial performance gains, as summarized in Table I (**bold** indicates the best result, and underline indicates the second-best). Specifically, ACT+eVGGT and DP+eVGGT achieve improvements of 2.1% and 6.5% over the original ACT and DP, respectively, highlighting the effectiveness of the encoded 3D knowledge in robotic policy learning. Notably, DP+eVGGT surpasses RDT by 1.2%, indicating that geometric representations can significantly improve non-pretrained policies, even outperforming large-scale pretrained methods using conventional vision encoders. While DP3 achieves the highest performance (23.4%) by using post-processed point clouds that remove walls and desks, the success rate of DP+eVGGT reaches a comparable 23.3% using only RGB inputs. This suggests that RGB-only policies with a strong geometry-aware encoder can approach the performance of point cloud-based methods without requiring post-processed data.

TABLE I
SUCCESS RATES ON ROBOTWIN SIMULATOR

Method	Modality	Beat Block Hammer			Adjust Bottle			Lift Pot			Place Burger Fries			Press Stapler			Handover Mic			Average		
		Seen	Unseen	Avg	Seen	Unseen	Avg	Seen	Unseen	Avg	Seen	Unseen	Avg	Seen	Unseen	Avg	Seen	Unseen	Avg	Seen	Unseen	Avg
DP3 [30]	Point cloud	0.08	<u>0.02</u>	0.050	0.62	0.30	<u>0.460</u>	0.10	<u>0.04</u>	0.070	0.18	<u>0.04</u>	0.110	0.15	<u>0.24</u>	<u>0.195</u>	0.72	0.32	0.520	0.308	<u>0.160</u>	0.234
RDT [24]	RGB	0.09	0.09	<u>0.090</u>	0.50	<u>0.35</u>	0.425	<u>0.12</u>	0.04	<u>0.080</u>	<u>0.20</u>	0.13	0.165	<u>0.20</u>	0.12	0.160	<u>0.61</u>	0.20	<u>0.405</u>	0.287	0.155	0.221
ACT [22]	RGB	0.07	0.00	0.035	0.16	0.12	0.140	0.03	0.01	0.020	0.04	0.00	0.020	0.02	0.02	0.020	0.02	0.00	0.010	0.057	0.025	0.041
ACT+eVGGT (ours)	RGB	0.07	0.01	0.040	0.20	0.10	0.150	0.02	0.02	0.020	0.10	0.00	0.050	0.14	0.03	0.085	0.04	0.01	0.025	0.095	0.028	0.062
DP [23]	RGB	0.14	0.01	0.075	0.46	0.24	0.350	0.06	0.02	0.040	0.16	0.04	0.100	0.18	0.09	0.135	0.50	0.12	0.310	0.250	0.087	0.168
DP+eVGGT (ours)	RGB	0.18	0.01	0.095	<u>0.52</u>	0.41	0.465	0.14	0.04	0.090	0.26	0.01	<u>0.135</u>	0.20	0.26	0.230	0.52	<u>0.24</u>	0.380	<u>0.303</u>	0.162	<u>0.233</u>

TABLE II

SUCCESS RATES ON MANISKILL SIMULATOR						
Method	Modality	Pick Cube	Push Cube	Stack Cube	Average	
DP [23]	RGBD	<u>0.95</u>	<u>0.92</u>	0.52	0.797	
RDT [24]	RGB	0.77	1.00	0.70	<u>0.823</u>	
ACT [22]	RGB	0.71	0.90	0.47	0.693	
ACT+eVGGT (ours)	RGB	0.75	0.89	0.49	0.710	
DP [23]	RGB	0.85	0.88	0.62	0.783	
DP+eVGGT (ours)	RGB	0.96	0.91	<u>0.65</u>	0.840	

Results on ManiSkill. Table II presents the effects of incorporating eVGGT into existing IL frameworks on ManiSkill. Notably, DP+eVGGT achieves the highest performance, outperforming RDT and DP with RGBD input by 1.7% and 4.3%, respectively. This result indicates that 3D spatial representations can support policy success rates at a level comparable to the pretrained knowledge utilized by RDT and the additional depth modality employed by DP. Similar to the results on RoboTwin, ACT+eVGGT and DP+eVGGT achieve average improvements of 1.7% and 5.7% over the original ACT and DP, respectively. Overall, our eVGGT encoder substantially strengthens performance across diverse manipulation settings.

TABLE III

COMPARISON WITH DIFFERENT VISION METHODS					
Method	Modality	Beat Block Hammer	Adjust Bottle	Average	
DP3 [30]	Point cloud from simulator	0.08	0.62	0.350	
DP3 [30]	Point cloud from eVGGT	0.04	0.25	0.145	
DP [23]+ResNet	RGB	0.14	0.46	0.300	
DP+ViT	RGB	0.12	0.37	0.245	
DP+eVGGT (ours)	RGB	0.18	<u>0.52</u>	0.350	

Comparison of Vision Methods. To evaluate the effectiveness of our proposed mechanism, which integrates the latent representation produced by eVGGT, we compare it with alternative vision methods for encoding visual information. Specifically, we additionally compare: *i*) using the point cloud produced by eVGGT, and *ii*) using a ViT backbone. We evaluate on two representative tasks: *Beat Block hammer* and *Adjust Bottle* on RoboTwin.

The results are summarized in Table III and reveal two key observations. First, DP3’s performance drops by 20.5% when using eVGGT point clouds, as DP3 depends on post-processed point clouds with clearly segmented objects, while eVGGT produces only unstructured data. This performance drop highlights that our implicit encoding design, which integrates scene geometry without requiring object-level segmentation, is more effective, since the latent representations provide useful geometric information for manipulation

policies. Second, among RGB-based encoders, DP+eVGGT achieves the highest performance, surpassing DP+ResNet by over 5% and DP+ViT by 11.5%, indicating that eVGGT captures geometry-aware scene dynamics more effectively. Notably, conventional DP employs ResNet, as ViT tends to underperform in low-data robotic settings, consistent with findings by Chi *et al.* [23].

B. Geometry-Aware Vision Encoder Evaluation

This section analyzes why using eVGGT as a vision encoder improves manipulation success. We study the efficiency of eVGGT and the geometric representations it learns, which together account for the observed performance gains. **Setup.** We evaluate 3D reconstruction performance on RoboTwin [18] and ManiSkill [19]. For RoboTwin, we train on the first 40 of 50 tasks and evaluate on the remaining 10 tasks, following the benchmark setup [18]. For ManiSkill, we train on *Stack Pyramid*, *Peg Insertion Side*, and *Push T*, and evaluate on a *Pick Cube*, *Push Cube*, and *Stack Cube*, similar to [49]. We measure performance on camera pose estimation, depth estimation, and 3D point cloud reconstruction on RoboTwin. For ManiSkill, since some tasks (for instance, *Pick Cube*, *Push Cube*) provide only single-view input, we focus on benchmarking depth estimation for consistency. Our knowledge distillation framework is trained on four NVIDIA A100 GPUs (40GB) over six days.

Baselines and Metrics. Our method is compared against VGGT [1] and DUST3R [9]. We choose DUST3R among geometry-grounded networks [8], [9] for comparison due to its well-balanced trade-off between 3D reconstruction accuracy and computational efficiency [50], making it a practical choice for real-world applications. We apply 300 refinement iterations for DUST3R following [9]. For camera pose estimation, we report Relative Pose Error (RPE), decomposed into translation (RPE_t) and rotation (RPE_r) components, which quantify deviations in relative position and orientation between predicted and ground-truth poses [51]. For depth estimation, we use *AbsRel*, the average of $|d_{\text{pred}} - d_{\text{gt}}|/d_{\text{gt}}$ over all pixels, and the δ metric, which measures the percentage of pixels where the predicted and ground-truth depths differ by 1.25-threshold, similar to [9]. For 3D point cloud reconstruction, we use Chamfer distance (CD) [5], a standard metric for the average distance between predicted and ground-truth points.

Efficiency Comparison. Table IV reports the efficiency of all three baselines. Our eVGGT considerably reduces model size by 5× and 2× compared to VGGT and DUST3R, respectively, achieves at least 9× faster inference, and lowers

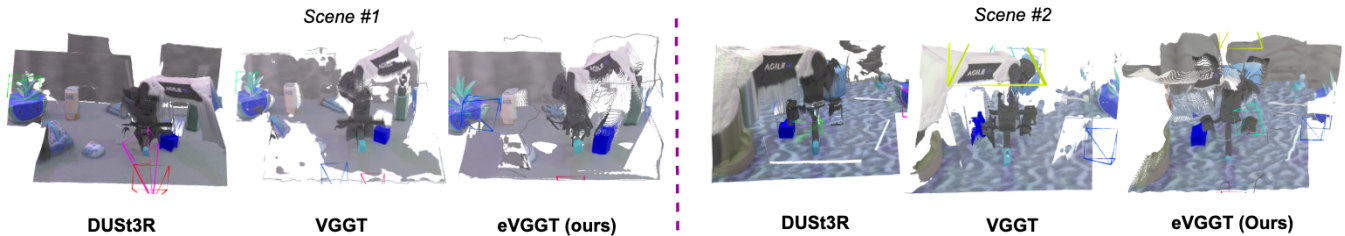


Fig. 6. **Qualitative 3D reconstruction results on RoboTwin.** Multi-view RGB inputs are provided to different geometry-grounded methods, and the corresponding reconstructed 3D scenes are visualized. We visualize two representative scenes from RoboTwin. **Note:** DUST3R’s point cloud requires post-processing with **300** refinement iterations. The ground-truth point cloud is sparse and colored by semantic labels; for clarity, it is not displayed.

TABLE IV

MODEL EFFICIENCY COMPARISON			
Method	Num. Params	Inference time (4 images)	Memory
VGGT [1]	1.29B	0.601s	7.2GB
DUST3R [9]	0.57B	5.248s	2.3GB
eVGGT (ours)	0.26B	0.069s	1.0GB

memory usage by 6.2GB and 1.3GB relative to VGGT and DUST3R, respectively. These results demonstrate that eVGGT is more suitable for scalable training as well as real-time robotic applications.

3D Reconstruction Results. Table V demonstrates that our eVGGT consistently outperforms DUST3R in 3D reconstruction on RoboTwin and ManiSkill. For camera pose estimation on RoboTwin, eVGGT achieves improvements of 0.097 in RPE_t and 3.89° in RPE_r over DUST3R, indicating more accurate pose reconstruction. In terms of depth estimation, eVGGT surpasses DUST3R on the δ metric by 11.5% on RoboTwin and 10.3% on ManiSkill. Our approach also achieves 3D reconstruction performance comparable to DUST3R, with a marginal CD gap of only 0.005 despite DUST3R’s costly refinement. We note, however, that since eVGGT is distilled from VGGT, its performance remains slightly below that of the teacher model.

TABLE V

3D RECONSTRUCTION ACCURACY IN SIMULATION							
Method	RoboTwin					ManiSkill	
	$RPE_t \downarrow$	$RPE_r \downarrow$	$AbsRel \downarrow$	$\delta \uparrow$	CD \downarrow	$AbsRel \downarrow$	$\delta \uparrow$
VGGT [45]	0.174	2.98°	0.702	0.689	0.104	0.403	0.608
DUST3R [9]	0.282	7.07°	1.137	0.513	0.107	0.498	0.485
eVGGT (ours)	<u>0.185</u>	<u>3.18°</u>	<u>0.827</u>	<u>0.628</u>	0.112	<u>0.445</u>	<u>0.588</u>

Qualitative Results. Fig. 6 presents reconstructed 3D scenes from RoboTwin. Our eVGGT achieves satisfactory reconstruction compared to other methods. In particular, the objects within the scene are correctly reconstructed, and the overall spatial arrangement is consistent and physically plausible. Furthermore, Fig. 7 illustrates depth estimation results on RoboTwin and ManiSkill. Our method outperforms DUST3R, particularly in challenging scenarios in RoboTwin, where DUST3R struggles to distinguish the wall from the desk. Similarly, in ManiSkill, DUST3R yields inconsistent depth estimates for the background wall, while both eVGGT and VGGT capture the gradual depth change.

Ablation Study on Training Components. We investigate how the components introduced in Sec. III-B, particularly

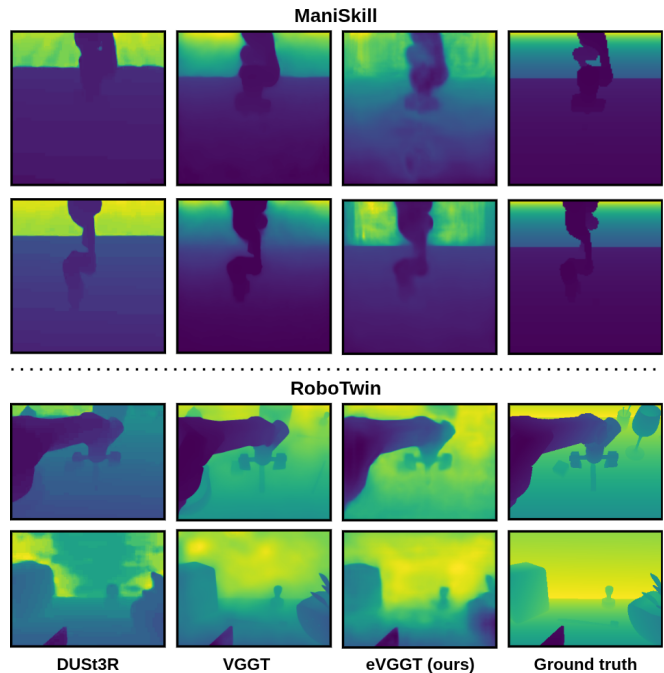
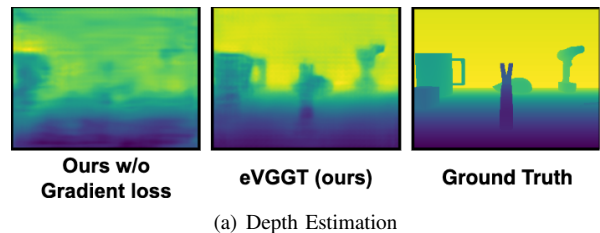
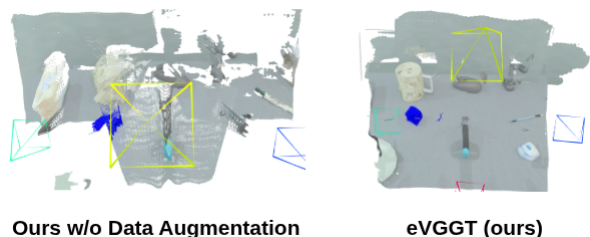


Fig. 7. **Depth estimation visualization.** Qualitative comparison of depth predictions from different geometry-grounded methods with the ground truth on RoboTwin and ManiSkill.



(a) Depth Estimation



(b) 3D Reconstruction

Fig. 8. **Qualitative ablation study results.**

the gradient loss (Eq. (2)) and the data augmentation strategy, contribute to the geometric reasoning capabilities of eVGGT. Empirically, the camera poses are learned reasonably well using the loss defined in Eq. (1); therefore, we focus on evaluating depth estimation and 3D point cloud reconstruction.

tion capabilities for our proposed framework. Table VI shows that removing the gradient loss significantly degrades performance ($AbsRel$ increases from 0.827 to 0.945, δ drops by 3.9%), highlighting its importance for smooth and consistent depth predictions (Fig. 8(a)). Omitting data augmentation also reduces 3D reconstruction accuracy (CD increases by 8.0%), demonstrating its role in improving generalization (Fig. 8(b)). These outcomes indicate that both components are crucial for accurate and robust 3D reconstruction.

TABLE VI

3D RECONSTRUCTION ABLATION			
Method	$AbsRel \downarrow$	$\delta \uparrow$	CD \downarrow
eVGGT (ours)	0.827	0.628	0.112
w/o grad. loss	0.945	0.589	0.128
w/o data aug.	0.866	0.614	0.121

TABLE VII

REAL-WORLD SUCCESS RATES		
Method	Push Cube	Pick Place Cube
DP [23]	0.54	0.40
DP+eVGGT (ours)	0.72	0.60

C. Real-World Robotic Experiments

Setup. For the real-robot evaluation, we focus on two single-arm manipulation tasks using a Kinova Gen3 robot: *i) Push Cube*, and *ii) Pick and Place Cube*, as shown in Fig. 9. We collect 10 human demonstrations per task via teleoperation using a 3Dconnexion SpaceMouse, allowing an operator to guide the robot end-effector in real time. To increase data diversity, we leverage MimicGen [52] to generate ≈ 2000 additional synthetic demonstrations for each task in a simulated RoboCasa [53] environment. This yields a large-scale training dataset featuring diverse scene configurations for the Kinova Gen3. In the dataset generation, we record three camera viewpoints during each demonstration: an eye-in-hand RGB camera on the robot’s wrist and two static third-person RGB cameras providing external views.

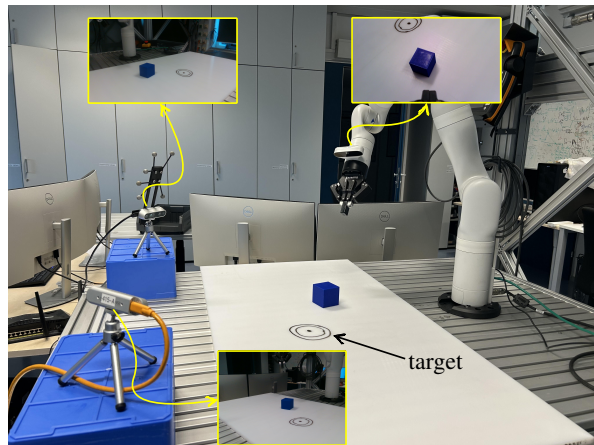


Fig. 9. **Robot Setup.** We conduct robot experiments with three camera views to push the cube to the target location.

Baselines. We train two policies: DP+eVGGT, using our geometry-aware encoder, and a DP [23] baseline with a conventional ResNet encoder. Both policies are trained on the same collected dataset. We evaluate 50 autonomous trials per task on hardware; a trial is successful if the cube is pushed past a target line (*Push Cube*) or the cube is placed within a 2 cm radius goal region (*Pick and Place Cube*).

Results. Table VII reports the real-world results. For *Push Cube*, DP+eVGGT achieves a **72%** success rate vs. **54%**

for the baseline. The gain is even greater in *Pick and Place Cube*, where DP+eVGGT reaches **60%** success vs. **40%** for the baseline. The geometry-aware encoder clearly improves performance in both tasks, indicating that better 3D understanding (via eVGGT) translates to more robust real-world manipulation performance. We provide a video of the real-robot experiments in the supplementary material.

D. Remarks

Tables I, II, and III show that using eVGGT as the vision encoder substantially improves manipulation success, achieving performance comparable to large-scale pretrained methods such as RDT [24] and approaches utilizing additional 3D information like DP3 [30] (Q1). The effectiveness of eVGGT emerges from its ability to capture rich 3D geometric information, enabling high-quality scene reconstruction (Table V, Figs. 6, and 7). Beyond its strong geometric reasoning capabilities, another key advantage of eVGGT is its efficiency (Table IV), which directly impacts practicality. Since policy training time scales with encoder runtime, the $9\times$ speedup makes extensive IL experiments feasible, which would be computationally prohibitive if using the full VGGT. Together, these factors explain eVGGT’s contribution to the success of robotic manipulation (Q2). Finally, real-robot evaluations (Table VII) show that the policy with our geometry-aware encoder successfully transfers from simulation to the real world, improving manipulation success rates (Q3).

V. DISCUSSION

We introduce eVGGT, a lightweight geometry-aware vision encoder that is significantly faster than existing visual geometry networks while preserving strong geometric reasoning capabilities. eVGGT can be seamlessly integrated into imitation learning baselines such as ACT and DP. Incorporating eVGGT yields substantial performance improvements, demonstrating its potential to serve as an effective alternative to traditional vision encoders in robotic manipulation.

Limitation. Although our proposed eVGGT achieves strong 3D reconstruction results and integrated policies show substantial improvements on RoboTwin and ManiSkill, the approach has notable limitations. First, its point clouds are dense and unstructured, which can reduce performance in 3D-based imitation learning baselines (Table III). Second, its 3D understanding remains implicit, serving mainly as a latent representation without explicitly linking robot actions to 3D scenes. Exploring this interesting direction will likely require large-scale pretraining on paired 3D observation–action data, which we leave for future work.

Broader Impact. We believe that integrating a geometry-aware vision encoder can substantially enhance the understanding of global 3D context in imitation learning, with potential applications extending beyond manipulation to other robotic tasks such as locomotion [31] and navigation [10]. Finally, efficiency is a key concern in the geometry-grounded literature, and other efforts [54] explore a similar direction. However, they do not focus on model size, which is critical for robotics due to hardware constraints.

REFERENCES

- [1] J. Wang, M. Chen, N. Karaev, A. Vedaldi, C. Rupprecht, and D. Novotny, "Vggt: Visual geometry grounded transformer," in *CVPR*, 2025.
- [2] Z. Xu, Q. Qiu, and Y. She, "Vilp: Imitation learning with latent video planning," *RA-L*, 2025.
- [3] S. An, Z. Meng, C. Tang, Y. Zhou, T. Liu, F. Ding, S. Zhang, Y. Mu, R. Song, W. Zhang, *et al.*, "Dexterous manipulation through imitation learning: A survey," *arXiv preprint arXiv:2504.03515*, 2025.
- [4] B. Tang, I. Akinola, J. Xu, B. Wen, A. Handa, K. Van Wyk, D. Fox, G. S. Sukhatme, F. Ramos, and Y. Narang, "Automate: Specialist and generalist assembly policies over diverse geometries," *RSS*, 2024.
- [5] A. Donat, X. Jia, X. Huang, A. Taranovic, D. Blessing, G. Li, H. Zhou, H. Zhang, R. Lioutikov, and G. Neumann, "Towards fusing point cloud and visual representations for imitation learning," in *ICLRW*, 2025.
- [6] V. Thengane, X. Zhu, S. Bouzerdoum, S. L. Phung, and Y. Li, "Foundational models for 3d point clouds: A survey and outlook," *arXiv preprint arXiv:2501.18594*, 2025.
- [7] G. Lu, S. Zhang, Z. Wang, C. Liu, J. Lu, and Y. Tang, "Manigaussian: Dynamic gaussian splatting for multi-task robotic manipulation," in *ECCV*, 2024.
- [8] R. Murai, E. Dexheimer, and A. J. Davison, "Mast3r-slam: Real-time dense slam with 3d reconstruction priors," in *CVPR*, 2025.
- [9] S. Wang, V. Leroy, Y. Cabon, B. Chidlovskii, and J. Revaud, "Dust3r: Geometric 3d vision made easy," in *CVPR*, 2024.
- [10] D. Maggio *et al.*, "Vggt-slam: Dense rgb slam optimized on the sl (4) manifold," *arXiv preprint arXiv:2505.12549*, 2025.
- [11] D. Zhuo, W. Zheng, J. Guo, Y. Wu, J. Zhou, and J. Lu, "Streaming 4d visual geometry transformer," *arXiv preprint arXiv:2507.11539*, 2025.
- [12] K. Wu, J. Zhang, H. Peng, M. Liu, B. Xiao, J. Fu, and L. Yuan, "Tinyvit: Fast pretraining distillation for small vision transformers," in *ECCV*, 2022.
- [13] Y. Xiong, B. Varadarajan, L. Wu, X. Xiang, F. Xiao, C. Zhu, X. Dai, D. Wang, F. Sun, F. Iandola, *et al.*, "Efficientsam: Leveraged masked image pretraining for efficient segment anything," in *CVPR*, 2024.
- [14] H. Ha, P. Florence, and S. Song, "Scaling up and distilling down: Language-guided robot skill acquisition," in *CoRL*, 2023.
- [15] R. He, S. Sun, J. Yang, S. Bai, and X. Qi, "Knowledge distillation as efficient pre-training: Faster convergence, higher data-efficiency, and better transferability," in *CVPR*, 2022.
- [16] W. Li, S. Shao, W. Liu, Z. Qiu, Z. Zhu, and W. Huan, "What role does data augmentation play in knowledge distillation?" in *ACCV*, 2022.
- [17] H. Wang, S. Lohit, M. N. Jones, and Y. Fu, "What makes a" good" data augmentation in knowledge distillation—a statistical perspective," *NeurIPS*, 2022.
- [18] T. Chen, Z. Chen, B. Chen, Z. Cai, Y. Liu, Q. Liang, Z. Li, X. Lin, Y. Ge, Z. Gu, *et al.*, "Robotwin 2.0: A scalable data generator and benchmark with strong domain randomization for robust bimanual robotic manipulation," *arXiv preprint arXiv:2506.18088*, 2025.
- [19] S. Tao *et al.*, "Maniskill3: Gpu parallelized robotics simulation and rendering for generalizable embodied ai," *RSS*, 2025.
- [20] S. Choi, S. Han, W. Kim, J. Chae, W. Jung, and Y. Sung, "Domain adaptive imitation learning with visual observation," *NeurIPS*, 2023.
- [21] A. Mandlekar, D. Xu, J. Wong, S. Nasiriany, C. Wang, R. Kulkarni, L. Fei-Fei, S. Savarese, Y. Zhu, and R. Martín-Martín, "What matters in learning from offline human demonstrations for robot manipulation," in *CoRL*, 2022.
- [22] T. Zhao, V. Kumar, S. Levine, and C. Finn, "Learning fine-grained bimanual manipulation with low-cost hardware," *RSS*, 2023.
- [23] C. Chi, Z. Xu, S. Feng, E. Cousineau, Y. Du, B. Burchfiel, R. Tedrake, and S. Song, "Diffusion policy: Visuomotor policy learning via action diffusion," *IJRR*, 2023.
- [24] S. Liu, L. Wu, B. Li, H. Tan, H. Chen, Z. Wang, K. Xu, H. Su, and J. Zhu, "Rdt-1b: a diffusion foundation model for bimanual manipulation," in *ICLR*, 2025.
- [25] D. Wang, C. Devin, Q.-Z. Cai, F. Yu, and T. Darrell, "Deep object-centric policies for autonomous driving," in *ICRA*, 2019.
- [26] M. Xu, Z. Xu, Y. Xu, C. Chi, G. Wetzstein, M. Veloso, and S. Song, "Flow as the cross-domain manipulation interface," in *CoRL*, 2025.
- [27] N. Di Palo and E. Johns, "Keypoint action tokens enable in-context imitation learning in robotics," in *RSS*, 2024.
- [28] Y. Zhu *et al.*, "Viola: Imitation learning for vision-based manipulation with object proposal priors," in *CoRL*, 2023.
- [29] Y. Qin, B. Huang, Z.-H. Yin, H. Su, and X. Wang, "Dexpoint: Generalizable point cloud reinforcement learning for sim-to-real dexterous manipulation," in *CoRL*, 2023.
- [30] Y. Ze, G. Zhang, K. Zhang, C. Hu, M. Wang, and H. Xu, "3d diffusion policy: Generalizable visuomotor policy learning via simple 3d representations," in *RSS*, 2024.
- [31] G. Xu, T. Wu, Z. Wang, Q. Wang, and F. Gao, "Flying on point clouds with reinforcement learning," *arXiv preprint arXiv:2503.00496*, 2025.
- [32] T. Hoang, H. Le, P. Becker, V. A. Ngo, and G. Neumann, "Geometry-aware rl for manipulation of varying shapes and deformable objects," in *ICLR*, 2025.
- [33] L. Zha, Y. Cui, L.-H. Lin, M. Kwon, M. G. Arenas, A. Zeng, F. Xia, and D. Sadigh, "Distilling and retrieving generalizable knowledge for robot manipulation via language corrections," in *ICRA*, 2024.
- [34] A. M. Mansourian, R. Ahmadi, M. Ghafouri, A. M. Babaei, E. B. Golezani, Z. Y. Ghamchi, V. Ramezani, A. Taherian, K. Dinashi, A. Miri, *et al.*, "A comprehensive survey on knowledge distillation," *arXiv preprint arXiv:2503.12067*, 2025.
- [35] A. Singh and H. Wang, "Simple unsupervised knowledge distillation with space similarity," in *ECCV*, 2024.
- [36] Q. Xiang, M. Zhang, Y. Shang, J. Wu, Y. Yan, and L. Nie, "Dkdm: Data-free knowledge distillation for diffusion models with any architecture," in *CVPR*, 2025.
- [37] H. Wu, D. Wu, T. He, J. Guo, Y. Ye, Y. Duan, and J. Bian, "Geometry forcing: Marrying video diffusion and 3d representation for consistent world modeling," *arXiv preprint arXiv:2507.07982*, 2025.
- [38] S. Lee, J. Choi, I. Kang, J. Kim, J. Park, and H. Shim, "3d-aware vision-language models fine-tuning with geometric distillation," *arXiv preprint arXiv:2506.09883*, 2025.
- [39] Y. Wang, H. Li, L.-p. Chau, and A. C. Kot, "Embracing the dark knowledge: Domain generalization using regularized knowledge distillation," in *ACM MM*, 2021.
- [40] M. Oquab *et al.*, "Dinov2: Learning robust visual features without supervision," *TLMR*, 2024.
- [41] T. Darcet, M. Oquab, J. Mairal, and P. Bojanowski, "Vision transformers need registers," in *ICLR*, 2024.
- [42] R. Ranftl, A. Bochkovskiy, and V. Koltun, "Vision transformers for dense prediction," in *ICCV*, 2021.
- [43] X. Puig *et al.*, "Habitat 3.0: A co-habitat for humans, avatars, and robots," in *ICLR*, 2024.
- [44] T. Yao, Y. Li, Y. Pan, and T. Mei, "Hiri-vit: Scaling vision transformer with high resolution inputs," *TPAMI*, 2024.
- [45] K. Tian, Y. Jiang, Z. Yuan, B. Peng, and L. Wang, "Visual autoregressive modeling: Scalable image generation via next-scale prediction," *NeurIPS*, 2024.
- [46] K. Xian, Z. Cao, C. Shen, and G. Lin, "Towards robust monocular depth estimation: A new baseline and benchmark," *IJCV*, 2024.
- [47] G. Jiang, Y. Sun, T. Huang, H. Li, Y. Liang, and H. Xu, "Robots pre-train robots: Manipulation-centric robotic representation from large-scale robot datasets," in *ICLR*, 2025.
- [48] J. Ho, A. Jain, and P. Abbeel, "Denoising diffusion probabilistic models," *NeurIPS*, 2020.
- [49] Z. Song, S. Qin, T. Chen, L. Lin, and G. Wang, "Physical autoregressive model for robotic manipulation without action pretraining," *arXiv preprint arXiv:2508.09822*, 2025.
- [50] J. Yang, A. Sax, K. J. Liang, M. Henaff, H. Tang, A. Cao, J. Chai, F. Meier, and M. Feiszli, "Fast3r: Towards 3d reconstruction of 1000+ images in one forward pass," in *CVPR*, 2025.
- [51] S. Li, Y. Gao, D. Sadigh, and S. Song, "Unified video action model," *RSS*, 2025.
- [52] A. Mandlekar *et al.*, "Mimicgen: A data generation system for scalable robot learning using human demonstrations," *CoRL*, 2023.
- [53] S. Nasiriany, A. Maddukuri, L. Zhang, A. Parikh, A. Lo, A. Joshi, A. Mandlekar, and Y. Zhu, "Robocasa: Large-scale simulation of everyday tasks for generalist robots," *RSS*, 2024.
- [54] Y. Shen, Z. Zhang, Y. Qu, and L. Cao, "Fastvggt: Training-free acceleration of visual geometry transformer," *arXiv preprint arXiv:2509.02560*, 2025.